# Heme interplay between IlsA and IsdC: Two structurally different surface proteins from [i]Bacillus[/i] cereus.

Elise Abi Khalil, Diego Segond, Tyson Terpstra, Gwenaëlle André-Leroux, Mireille Kallassy, Didier Lereclus, Fadi Bou-Abdallah, Christina Nielsen-Leroux

Biochimica et Biophysica Acta 1850 (2015) 1930–1941

Contents lists available at ScienceDirect

Biochimica et Biophysica Acta

journal homepage: www.elsevier.com/locate/bbagen

# Heme interplay between IlsA and IsdC: Two structurally different surface proteins from *Bacillus cereus*

Elise Abi-Khalil [a,b,c,1], Diego Segond [a,1], Tyson Terpstra [c], Gwenaëlle André-Leroux [d], Mireille Kallassy [b], Didier Lereclus [a], Fadi Bou-Abdallah [c,*], Christina Nielsen-Leroux [a,*]

[a] INRA, UMR 1319 Micalis-AgroParisTech, AgroParisTech UMR Micalis, F-78352 Jouy en Josas, France
[b] Laboratory of Biotechnology, Saint-Joseph University, Beyrouth, Lebanon
[c] Department of Chemistry, State University of New York at Potsdam, Potsdam, NY 13676, USA
[d] INRA, MIG, Domaine de Vilvert, F-78352 Jouy en Josas, France

ARTICLE INFO

*Article history:*
Received 27 April 2015
Received in revised form 4 June 2015
Accepted 16 June 2015
Available online 18 June 2015

*Keywords:*
Hemin binding
IlsA NEAT domain
Hemoglobin
Kinetics
LRR domain

ABSTRACT

*Background:* Iron is an essential element for bacterial growth and virulence. Because of its limited bioavailability in the host, bacteria have adapted several strategies to acquire iron during infection. In the human opportunistic bacteria *Bacillus cereus*, a surface protein IlsA is shown to be involved in iron acquisition from both ferritin and hemoproteins. IlsA has a modular structure consisting of a NEAT (Near Iron transporter) domain at the N-terminus, several LRR (Leucine Rich Repeat) motifs and a SLH (Surface Layer Homology) domain likely involved in anchoring the protein to the cell surface.
*Methods:* Isothermal titration calorimetry, UV–Vis spectrophotometry, affinity chromatography and rapid kinetics stopped-flow measurements were employed to probe the binding and transfer of hemin between two different *B. cereus* surface proteins (IlsA and IsdC).
*Results:* IlsA binds hemin via the NEAT domain and is able to extract heme from hemoglobin whereas the LRR domain alone is not involved in these processes. A rapid hemin transfer from hemin-containing IlsA (holo-IlsA) to hemin-free IsdC (apo-IsdC) is demonstrated.
*Conclusions:* For the first time, it is shown that two different *B. cereus* surface proteins (IlsA and IsdC) can interact and transfer heme suggesting their involvement in *B. cereus* heme acquisition.
*General significance:* An important role for the complete Isd system in heme-associated bacterial growth is demonstrated and new insights into the interplay between an Isd NEAT surface protein and an IlsA-NEAT-LRR protein, both of which appear to be involved in heme-iron acquisition in *B. cereus* are revealed.


## 1. Introduction

Iron is an essential element for most living organisms and can be found in complex with host proteins such as hemoglobin, ferritin and transferrin [1]. Pathogenic bacteria have developed a number of strategies involving various iron and heme acquisition and uptake systems including a network of surface and membrane proteins found in both Gram-positive and Gram-negative bacteria. While extracellular hemophores bind to outer membrane receptors in Gram-negative bacteria, several Gram-positive pathogens such as *Listeria monocytogenes*, *Staphylococcus aureus* and *Bacillus anthracis* use peptidoglycan bound Iron surface determinants (Isd) of which the Near Iron Transporter domains (NEAT) can bind and acquire heme [2,3]. In the human opportunistic pathogen *Bacillus cereus* (*B. cereus*), which is closely related to *B. anthracis* [4–6], an iron regulated leucine rich repeat surface protein "IlsA" (gene number BC1331) has been identified and shown to directly bind heme, hemoglobin and ferritin [7,8]. IlsA has a unique structure with three different domains: NEAT, LRR (Leucine Rich Repeat) and SLH (S-Layer homology). Under iron limiting conditions, the bacterial surface protein IlsA, which is likely anchored to the peptidoglycan is produced and can interact with the aforementioned host iron molecules [8]. Although NEAT domains are known for their heme binding affinity, they can exhibit discrepancy in their specificity. For instance, some NEAT-proteins act as hemoglobin receptors, others strictly bind heme but almost all take part in the network of NEAT domains mediating heme transfer from the bacterial surface to the bacterial membrane [9,3]. The LRR domains are composed of consecutive structural units that provide a large surface of interaction making them an ideal motif for protein–protein interactions [10,11]. To date, the role of LRR in heme binding has not been described but recent work from our laboratory suggested an interaction between the iron storage protein ferritin and the LRR domain alone.

Here, using several biochemical and *in vitro* approaches, we first characterized the ability of full-length IlsA, the individually expressed and purified NEAT and LRR domains and a NEAT domain mutated full-length IlsA

* Corresponding authors.
[1] Shared first authorship.

http://dx.doi.org/10.1016/j.bbagen.2015.06.006
0304-4165/

to bind hemin. Secondly, we looked into a possible role of the *B. cereus* Isd system in interaction with IlsA to bind and transfer hemin. Our results indicate that IlsA binds hemin via the NEAT domain and is able to extract heme from hemoglobin whereas the LRR domain alone is not involved in these processes. Moreover, we demonstrate an important role for the complete Isd system in heme-associated bacterial growth and provide new insights into the interplay between an Isd NEAT surface protein and an IlsA-NEAT-LRR protein, both of which appear to be involved in heme-iron acquisition in *B. cereus*.

## 2. Results and discussion

### *2.1. Roles of $NEAT_{IlsA}$ and $LRR_{IlsA}$ domains in hemoglobin binding and heme extraction*

The NEAT and LRR domains of IlsA (Fig. 1A) probably confer to the protein an ability to bind different iron sources (i.e. hemoglobin, hemin and ferritin). NEAT domains from various Isd proteins are implicated in heme binding meanwhile a role for LRR in heme binding has not been demonstrated nor proposed. We thus presumed it might be involved in protein binding. To examine the ability of different domains of IlsA to bind hemoglobin, several heme-free apo-proteins were prepared (i.e. IlsA, $NEAT_{IlsA}$, $LRR_{IlsA}$) by constructing recombinant proteins overexpressed and purified from a non-heme-producing *Escherichia coli* strain (C600 Δ*hemA*). A direct interaction between IlsA and human hemoglobin (Hb) has already been reported [8] but it is not known whether the binding is transitory or if IlsA is able to extract heme from Hb. The role of LRR in Hb binding is also unknown. To investigate these possible interactions, glutathione–sepharose gel loaded with either GST-apo-IlsA, GST-apo-$NEAT_{IlsA}$ or GST-$LRR_{IlsA}$ was incubated in the presence or absence of Hb. The sepharose gel was then centrifuged to separate bound heme (stuck to the GST-tagged molecules) from the supernatant containing free Hb with more or less heme. No absorbance in the 400 nm range was observed when GST-IlsA, GST-$NEAT_{IlsA}$ or GST-$LRR_{IlsA}$ gel bound fractions were eluted with reduced glutathione in the absence of Hb (Fig. 1B, C and D, blue curves). Following incubation with Hb, both GST-IlsA and GST-$NEAT_{IlsA}$ displayed a spectrum at 404 nm characteristic of hemin-binding proteins (Fig. 1B and C, green curves) whereas no Soret peak was observed in the experiments performed with GST-$LRR_{IlsA}$ (Fig. 1D, green curves). To ensure that the change in the visible spectra was not due to hemoglobin bound to GST-protein, the different fractions (supernatant and sediment) were analyzed by SDS PAGE. Only one band per fraction corresponding to either the GST-protein or hemoglobin was observed (data not shown), thus confirming that the change in absorption is a result of heme transfer. The 404 nm heme peak of Hb decreased after incubation with apo-IlsA suggesting that IlsA had extracted heme from Hb (Fig. 1B, red curve). The apo-$NEAT_{IlsA}$ was also shown to extract heme from Hb (red curve) albeit less efficiently compared to the wild type protein (Fig. 1C, red curve). On the contrary, the absorbance spectrum of Hb remained essentially unchanged after incubation with the LRR domain of IlsA (Fig. 1D, red and black curves). These results are in line with the absence of Soret peak for the GST-$LRR_{IlsA}$ incubated with Hb. Altogether, our data indicate that the LRR domains alone of IlsA are unable to bind to Hb and extract heme from Hb and that the $NEAT_{IlsA}$ domain is involved in both Hb binding and heme extraction from Hb. Ekworomadu et al. [19] attributed the direct association of Hb with *B. anthracis* IsdX1 to Ser-53 since mutation of this residue led to a loss of Hb binding. This observation was supported by an earlier X-ray structure of *S. aureus* IsdH in complex with the alpha-chain of Hb showing a hydrogen bond between Ser-130 on IsdH NEAT and Lys-11 on Hb [20]. This residue (Ser-61 for IlsA) is highly conserved in the $3_{10}$ helix of many NEAT domains (Fig. 2A). A more recent study [15] identified Gln-29 in IsdX2 of *B. anthracis* as a critical residue for heme extraction from methemoglobin. When Gln-29 is mutated to Thr, the protein lost its ability to extract heme. Significantly, Gln-29 which belongs to the

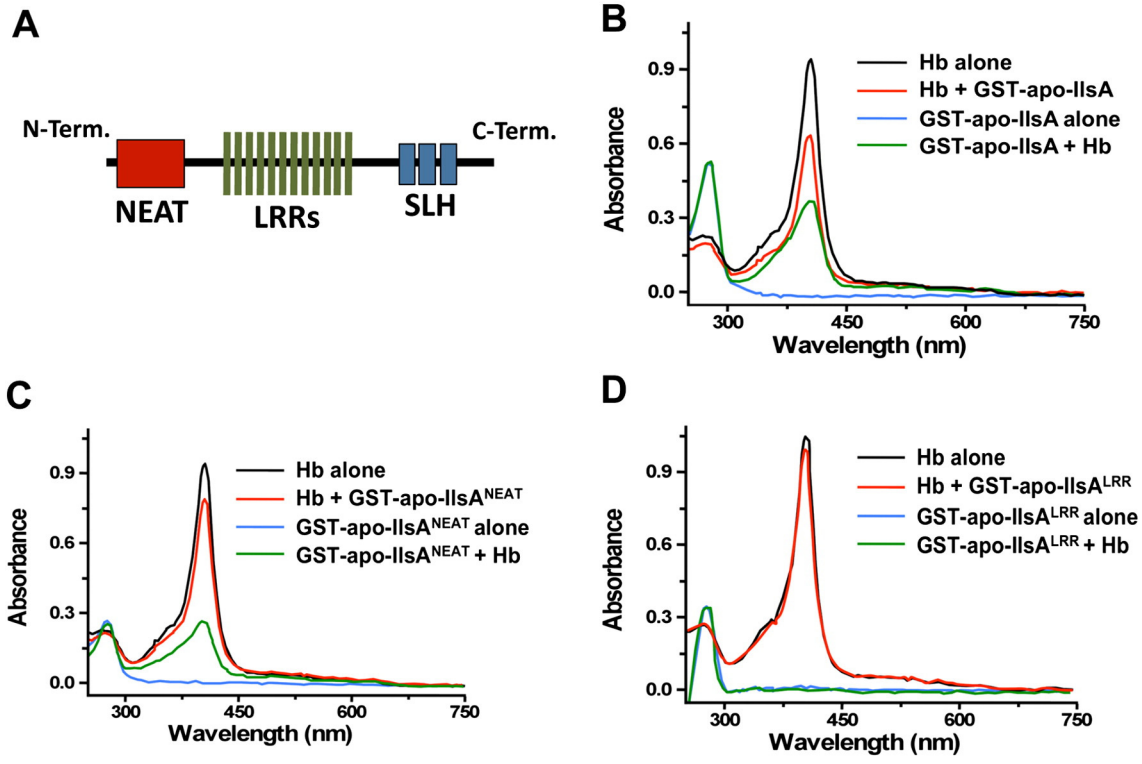


**Fig. 1.** Heme extraction from hemoglobin by the NEAT domain of IlsA. (A) Predicted modular structure of the protein IlsA showing the NEAT (139 amino acids) and the LRR (285 amino acids) domains (B) GST-apo-IlsA (20 μM), (C) GST-apo-$NEAT_{IlsA}$ (20 μM) and (D) GST-$LRR_{IlsA}$ (10 μM) were anchored to glutathione–sepharose and incubated with hemoglobin (5 μM) for 30 min at 25 °C. Comparison of the absorbance spectra of hemoglobin before (black curves) and after association with (B) GST-apo-IlsA, (C) GST-$NEAT_{IlsA}$ or (D) GST-$LRR_{IlsA}$ (red curves) and of (B) GST-apo-IlsA, (C) GST-apo-$NEAT_{IlsA}$ or (D) GST-$LRR_{IlsA}$ before (blue curves) and after incubation with hemoglobin (green curves).

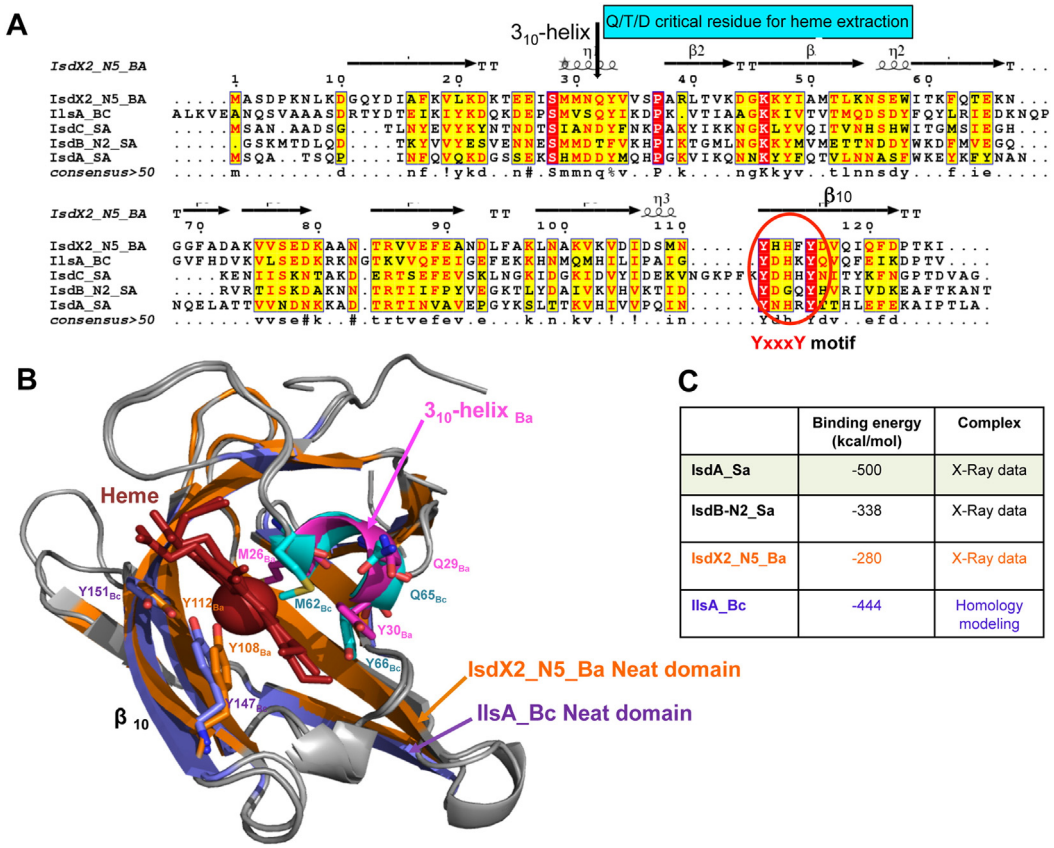


| | Binding energy (kcal/mol) | Complex |
|---|---|---|
| IsdA_Sa | -500 | X-Ray data |
| IsdB-N2_Sa | -338 | X-Ray data |
| IsdX2_N5_Ba | -280 | X-Ray data |
| IlsA_Bc | -444 | Homology modeling |

**Fig. 2.** Structural comparison of NEAT domains. (A) Two-dimensional alignment of IlsA NEAT domain from *B. cereus* (Bc) with the NEAT 5 domain of IsdX2 from *B. anthracis* (reference 4HP8 fasta and pdb) and the NEAT domains from IsdC, IsdB_N2 and IsdA from *S. aureus* (the numbering arbitrarily starts at Met1 for IsdX2_N5_Ba). (B) Structural overlay of the homology model of the IlsA-Bc NEAT domain (purple β-sheets and cyan $3_{10}$ helix) and the *B. anthracis* NEAT 5 domain of IsdX2 (orange β-sheets and pink $3_{10}$ helix). Heme docking is highlighted in red sticks alongside residues involved in heme binding. The numbering of residues with subscripts Ba and Bc refer to *B. anthracis* and *B. cereus*, respectively. The image was generated using PyMol (www.pymol.org). (C) Binding energies computed for the holo-structures of the NEAT domains (from pdb) and IlsA-Bc NEAT domain in complex with heme as determined by homology modeling.

$3_{10}$ helix is conserved in IlsA-Bc (Fig. 2A) and corresponds to Gln-65 in Fig. 2B.

Our experimental data combined with the homology model suggest that IlsA association with Hb and heme extraction may involve Ser-61 and Gln-65 and that these residues might play a critical role in Hb binding and heme extraction similarly to Ser-53 in IsdX1 and Gln-29 in IsdX2. However, a role of the LRR domain in hemoglobin binding cannot be precluded in the present study since it might stabilize the protein–hemoglobin complex.

### 2.2. The relative roles of $NEAT_{IlsA}$ and $LRR_{IlsA}$ domains in hemin binding

To closely examine the binding characteristics of hemin with full length IlsA, the NEAT and the LRR domains alone, the purified proteins

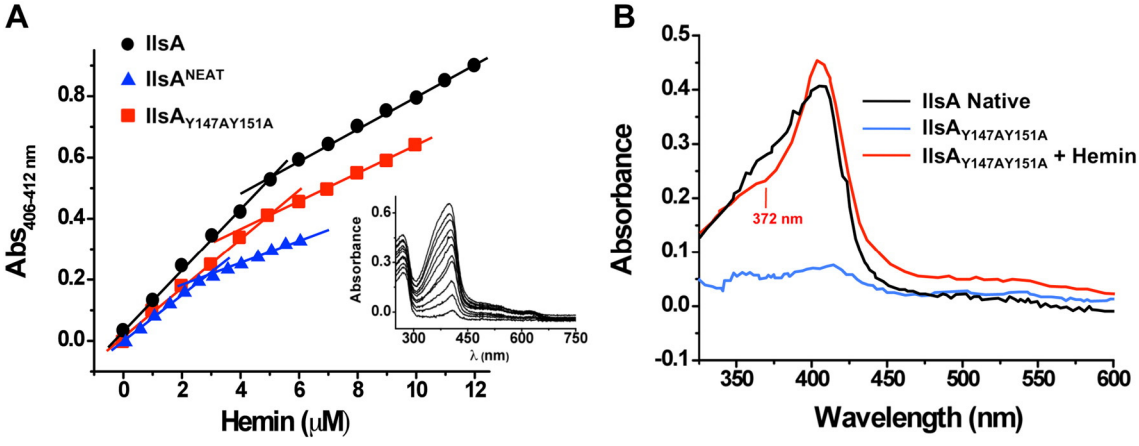


**Fig. 3.** Hemin binding to apo-IlsA, apo-$NEAT_{IlsA}$ and $IlsA_{Y147AY151A}$. (A) Spectrophotometric titrations of apo-IlsA, apo-$NEAT_{IlsA}$ and $IlsA_{Y147AY151A}$ with exogenous hemin. 4.3 μM apo-IlsA (black circles), 5 μM $IlsA_{Y147AY151A}$ (red squares) were titrated with 1 μM hemin per injection and 2.5 μM apo-$NEAT_{IlsA}$ (blue triangles) was titrated with 0.5 μM hemin per injection. All protein solutions were prepared in 50 mM Tris, 150 mM NaCl, pH 7.4 and 25 °C. The inset shows an example titration curve with full-length IlsA. (B) Absorbance spectra of 5 μM protein solutions produced in *E. coli* M15; native IlsA (black curve), alanine-substitution mutant $IlsA_{Y147AY151A}$ (blue curve) and $IlsA_{Y147AY151A}$ in presence of 5 μM hemin (red curve).

were submitted to spectrophotometric titration studies. The addition of hemin to a full-length apo-IlsA protein led to an increase in the Soret band at 407 nm characteristic of a protein-heme complex. A plot of the maximum absorbance at 407 nm as a function of hemin concentration revealed a binding stoichiometry of one hemin per protein for native full-length IlsA (Fig. 3A, black circles). Similarly, titration of a 2.5 μM apo-$NEAT_{IlsA}$ domain alone with an increased amount of hemin showed saturation at ~2.6 μM of hemin (Fig. 3A, blue triangles) indicating again a binding stoichiometry of one hemin per one $NEAT_{IlsA}$. However, $LRR_{IlsA}$ domain alone did not exhibit any peaks in the ~400 nm region following excess addition of hemin (data not shown). These results suggest that the NEAT domain mediates hemin binding to IlsA and that the LRR domain alone is not involved in hemin binding, (at least under our experimental conditions) in accord with the prior results showing lack of binding to hemoglobin.

### 2.3. Role of IlsA NEAT domain residues Tyr-147 and Tyr-151 in hemin binding

We have now shown that for IlsA, the NEAT domain is essential for hemoglobin and hemin binding. However, the identity of the amino acids or the heme binding region on IlsA is still lacking. NEAT domains from various Isd proteins are implicated in heme binding and crystallographic studies of IsdA of *S. aureus* showed that heme binding and coordination are due to a conserved tyrosine Tyr-166 that is involved in hydrogen-bonding with Tyr-170 [12]. Multiple sequence alignments of NEAT domains of IlsA with Isd proteins from *S. aureus* (Sa) and *B. anthracis* (Ba) identified two tyrosine residues (Tyr-147 and Tyr-151, IlsA numbering) from the highly conserved motif YxxxY which align with Tyr-166 and Tyr-170 in IsdA-Sa, Tyr-440 and Tyr-444 in IsdB-N2-Sa, Tyr-132 and Tyr-136 in IsdC-Sa and Tyr-108 and Tyr-112 in IsdX2-Ba (Fig. 2A). The YxxxY motif is involved in heme binding, with one of the tyrosine providing the fifth axial ligand for the iron-heme coordination and the other forming a hydrogen bond that strengthens heme coordination [12–15]. To study the role of the conserved tyrosines in IlsA, a homology model for the NEAT domain of IlsA is computed and superimposed with IsdX2-N5-Ba used here as a template (Fig. 2B). The model indicates that Tyr-147 and Tyr-151 of IlsA NEAT domain are part of the heme binding pocket. In addition, site-directed mutagenesis of the conserved heme-iron coordinating residues Tyr-147 and Tyr-151 to alanine (variant $IlsA_{Y147AY151A}$) resulted in a drastic decrease in the absorbance at 407 nm ($A_{407\ nm} = 0.03$) and a 5-fold reduction in the amount of hemin bound to $IlsA_{Y147AY151A}$ in comparison to the full-length wild type IlsA (Fig. 3B), indicating an important role of Tyr-147 and Tyr-151 in hemin binding. While unable to efficiently bind intracellular heme in *E. coli*, variant $IlsA_{Y147AY151A}$ was shown to bind exogenous hemin with a 1:1 stoichiometry (Fig. 3A, red squares) suggesting that other residues might be involved in hemin binding. However, the UV–Vis spectrum of the $IlsA_{Y147AY151A}$-hemin complex shows a shoulder at around 372 nm indicative of a perturbation in the heme binding pocket (Fig. 3B, red curve). Interestingly, the heme binding pocket of IlsA-Bc is located at the interface between strand β10 and $3_{10}$-helix with Tyr-147 and Tyr-151 of strand β10 and Met-62, Gln-65 and Tyr-66 of $3_{10}$-helix strictly aligning with Tyr-108 and Tyr-112 and Met-26, Gln-29 and Tyr-30 of IsdX2-Ba, respectively (Fig. 2B). To estimate the binding energy, based on the homology modeling with crystallized NEAT domains from Isd proteins, docking experiments were performed. The results confirm heme coordination to those five residues with binding energy similar to the crystallized complexes (Fig. 2C). Moreover, a recent study showed that a single mutation of the distal loop residues was insufficient to perturb the IsdA-heme complex in *S. aureus* and that mutation of the heme-iron ligand Tyr-166 was compensated for by His-83 [16]. In *B. cereus* IlsA, His-83 is replaced by Met-62 and the X-ray crystal structure of the *S. aureus* IsdB-N2-heme showed that Met-363 (which aligns with Met-62 of IlsA) is involved in iron-heme coordination [13] raising the possibility that Met-62 of IlsA might also be involved in heme binding. Our results show that both the full-length wild type IlsA and variant $IlsA_{Y147AY151A}$ bind exogenous hemin. However, while variant $IlsA_{Y147AY151A}$ almost completely lost its affinity for endogenous hemin, it maintained a weak affinity to exogenous hemin presumably via Met-62, Gln-65 and Tyr-66 located within the hydrophobic heme binding pocket (Fig. 2B). The observed differences between endogenous versus exogenous hemin might be due to differences between actual heme concentration in *E. coli* and the much higher non-physiological hemin concentrations employed in our *in vitro* studies. Alternatively, it is possible that the reduced affinity of $IlsA_{Y147AY151A}$ for hemin prevents competition with other *E. coli* hemoproteins during protein production.

### 2.4. Kinetics of hemin association to IlsA and $NEAT_{IlsA}$

In order to compare the hemin binding kinetics between full-length IlsA and the $NEAT_{IlsA}$ domain alone, absorbance time curves were collected on a rapid kinetics stopped-flow equipment. Fig. 4 illustrates the absorbance-time curves at 410 nm and the family of UV–Vis spectra (insets) for hemin association to apo-IlsA (Fig. 4A) and apo-$NEAT_{IlsA}$ (Fig. 4B). The time course at $A_{410\ nm}$ for both proteins could be described by two exponential equations resulting in two rate constants, $k_1$ (fast) and $k_2$ (slow) ($49.4 \pm 4.6\ s^{-1}$ and $2.9 \pm 0.3\ s^{-1}$ for full-length IlsA and $52.7 \pm 5.1\ s^{-1}$ and $2.3 \pm 0.2\ s^{-1}$ for $NEAT_{IlsA}$) with the two kinetic steps contributing equally to the total spectral change (Fig. 4C). A recent investigation [17] of an aqueous ferriprotoporphyrin IX reported the presence of monomeric and dimeric hemin species in solution and that dimeric hemin consisted of non-covalent interaction between two monomer subunits. The rapid phase observed in our kinetics data can be attributed to the reaction of monomeric hemin with apo-IlsA whereas the slower kinetic phase corresponds to the dissociation of dimeric hemin followed by the rapid association of the resulting monomeric hemin with the protein. Similar hemin association kinetics have been previously described with *S. aureus* apo-IsdA [18].

### 2.5. Roles of B. cereus isd locus and isdC mutants in iron acquisition from hemin and hemoglobin

Because IlsA alone is unlikely to be involved in heme binding, transport and release, we sought first to investigate the role of the whole *isd* locus, not yet explored in *B. cereus*, in hemin uptake and transport. We then examined the interaction of holo-IlsA with Bc4549 (the first protein of the *isd* locus, here referred to as *isdC*) in order to explore the ability of IlsA to transfer hemin to IsdC. The *isd* locus is composed of eight open reading frames (Fig. 5A) encoding for three NEAT proteins (Bc4549, Bc4548 and Bc4547), a possible iron permease system (Bc4546, Bc4545, Bc4544), a putative sortase (Bc4543) and a putative mono-oxygenase (Bc4542) that degrades heme to liberate iron into the cytosol. Bc4549 and Bc4547 are believed to be two surface proteins because of their sortase motifs: NPKTG and NSKTA, respectively. In contrast, Bc4548 lacks a clear anchoring motif and might act as a secreted hemophore. *In silico* analysis showed a high similarity between the *isd* operons of *B. anthracis* and *B. cereus*. IsdC and IsdX1 from *B. anthracis* share 98% sequence identity with Bc4549 and Bc4548 respectively compared to 86% for IsdX2 and Bc4547 [21,22].

First, to study the relative importance of Isd and IlsA in growth with heme irons sources the growth rates of the wild type (Bc ATCC14579), Δ*ilsA*, Δ*isd* and Δ*ilsA*Δ*isd* strains were compared under different experimental conditions of LB iron-depleted medium with or without hemoglobin or hemin. The *isd* locus mutant showed a remarkable growth defect ($p < 0.05$) when cultivated in the presence of hemin and hemoglobin as sole iron sources but no significant difference in growth ($p > 0.05$) between the *isd* locus mutant and the double mutant Δ*ilsA* Δ*isd* was detected (Fig. 5C and D), suggesting that components of the *isd* locus have a significant role in iron scavenging from hemoproteins. To examine the possible cooperation between IlsA and the first protein of the *isd* operon (presumably a peptidoglycan located protein) in heme

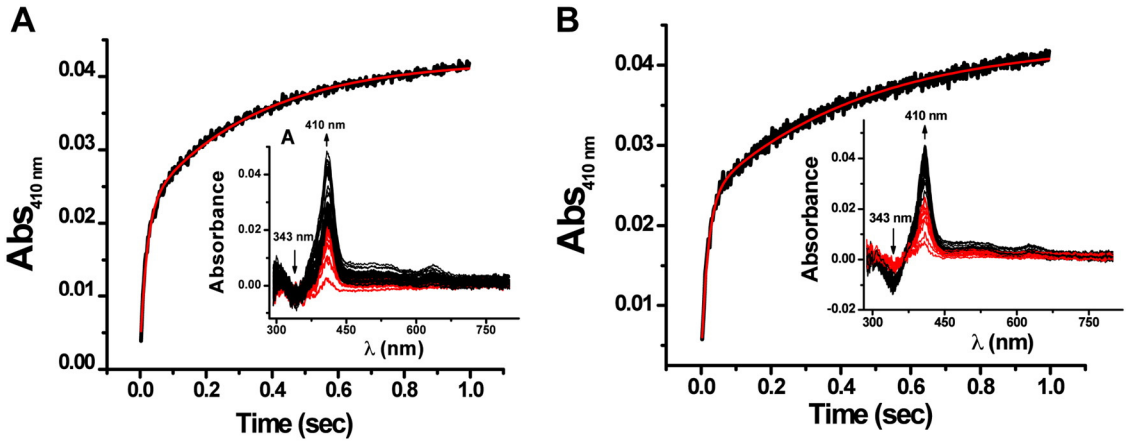


C

| Apo-proteins + Hemin | $A_1$ | $k_1$ ( $s^{-1}$) | $A_2$ | $k_2$ ( $s^{-1}$) |
|---|---|---|---|---|
| Apo-IlsA C600 | 0.0196 ± 0.0022 | 49.4 ± 4.6 | 0.0203 ± 0.0012 | 2.9 ± 0.3 |
| Apo-IlsA-NEAT | 0.0204 ± 0.0024 | 52.7 ± 5.1 | 0.0195 ± 0.0006 | 2.3 ± 0.2 |

**Fig. 4.** Absorbance time curves at 410 nm for hemin association with apo-IlsA and apo-$NEAT_{IlsA}$. (A) 15 μM apo-IlsA or (B) apo-$NEAT_{IlsA}$ and 10 μM hemin; both protein solutions were in 50 mM Tris, 150 mM NaCl, pH 7.4 and 25 °C. The red curves are the best fit to the experimental data in black using two exponential equations. The insets are the family of stopped-flow UV–Vis spectra gathered every 2.5 ms for the first 40 ms (red) of the reaction and every 50 ms (black) thereafter. (C) First order rate constants ($k_1$ and $k_2$) and the corresponding absorbance values ($A_1$ and $A_2$); both proteins are produced in *E. coli* C600 and presumed to be heme free.

transport and iron acquisition, a Δ*isdC* mutant was analyzed. Compared to the wild type, the growth of the Δ*isdC* mutant was not affected in an iron-depleted medium enriched by hemin or hemoglobin (Fig. 5C and D). In fact, under our *in vitro* conditions the deletion of *ilsA* or *isdC* alone did not lead to a strong phenotype in contrast to the whole locus mutant (Table S1). These data suggest a certain level of functional redundancy among the Isd components. Interestingly, and despite relative homology in the iron acquisition systems between *B. cereus* and *B. anthracis*, our study highlights significant differences in growth. For instance, the *B. anthracis* Δ*isdC* mutant exhibited a small growth defect when grown in an iron-free medium supplemented with hemin [21] whereas the newly identified *B. anthracis* Hal protein (a protein similar to IlsA with a NEAT domain and several LRRs) had an apparent stronger role than *isd* compounds in growth with hemin and hemoglobin as sole iron sources [23]. In fact, the current study suggests that IlsA does not have a strong role in heme iron uptake as reported earlier [8] presumably because tetracycline was used as a selection marker in the growth medium in our earlier study. Tetracycline can act as an iron chelator [24], thus interfering with iron availability. Moreover, the efflux pump encoded by the tetracycline resistance cassette inserted in the Δ*ilsa* strain required divalent cations to function [25]. Consequently, without iron readily available (i.e. not in complex with hemoproteins), the efflux pump might not remove efficiently tetracycline from the bacterial cells, resulting in growth inhibition. Therefore, our current data suggest that IlsA plays a minor role in heme and hemoglobin uptake and that the Isd heme-iron acquisition system is more strongly involved in *B. cereus* heme-iron uptake, with or without the assistance of IlsA. Nevertheless, the relative importance of IlsA and Isd system in heme-iron uptake might vary depending on the iron sources available in the host tissues.

### 2.6. Hemin association with IsdC: binding stoichiometry and rate of reaction

Although the Δ*isdC* mutant was not affected in growth with heme sources, we cannot preclude a possible role in heme binding and transfer at the bacterial surface. Because our data indicate that IlsA can bind hemoglobin and also extract heme from different heme sources, we hypothesize that it could also transfer heme to another NEAT domain molecule like IsdC. We therefore tested the ability of IsdC to bind hemin. Recombinant IsdC was purified either in *E. coli* strains M15 (to obtain holo-IsdC) or in C600Δ*hemA* (to obtain the apo-form) and hemin binding characteristics of IsdC were then compared to those of wild type IlsA. Our results show that holo-IsdC possesses the characteristics of a heme-binding protein with a Soret peak at 410 nm in addition to a series of Q bands in the visible region at 511, 549, 570 and 624 nm (Fig. S1). Multiple sub-stoichiometric additions of hemin to apo-IsdC revealed a binding stoichiometry of 1 apo-Isd protein per 1 hemin molecule (Fig. 6A). Stopped-flow spectrophotometric measurements of hemin association with apo-IsdC showed a maximal change in the absorbance at ~408 nm and a double exponential fit to the data yielded two rate constants $k_1 = 58.9 \pm 6.2\ s^{-1}$ and $k_2 = 5.7 \pm 0.5\ s^{-1}$ (Fig. 6B and C), similarly to those found with IlsA and $NEAT_{IlsA}$. Thus, the purified IsdC is capable of binding hemin with more or less the same rate constant as IlsA.

### 2.7. Thermodynamics of holo-IlsA interaction with apo-IsdC

Assuming heme transfer from IlsA to IsdC takes place, an interaction between these two molecules would be expected and one of the most direct ways of evaluating interactions between biological molecules is ITC (isothermal titration calorimetry). Fig. 7 shows the injection heats for apo-IsdC binding to holo-IlsA at pH 7.0 and 25.00 °C and the integrated heats (μJ) for each injection *vs* the molar ratio of apo-IsdC to holo-IlsA after subtraction of the control heats. The positive upward peaks in Fig. 7A correspond to an exothermic reaction with a binding stoichiometry of ~1 apo-IsdC protein per holo-IlsA and a dissociation constant of ~312 nM. The interaction between the two proteins was achieved with both favorable enthalpy and entropy changes. Moreover, additions of apo-IlsA to apo-IsdC yielded heats similar to the control experiment suggesting that heme is required for the association of holo-IlsA to apo-IsdC (data not shown). All the experimental thermodynamic parameters were obtained from curve fitting of the integrated heats using a model of one set of independent binding sites and are compiled in Fig. 7C. The $K_d$ value of ~312 nM for holo-IlsA and apo-IsdC is well within the range of published values in other systems. For instance, binding experiments between HasA, an extracellular heme binding

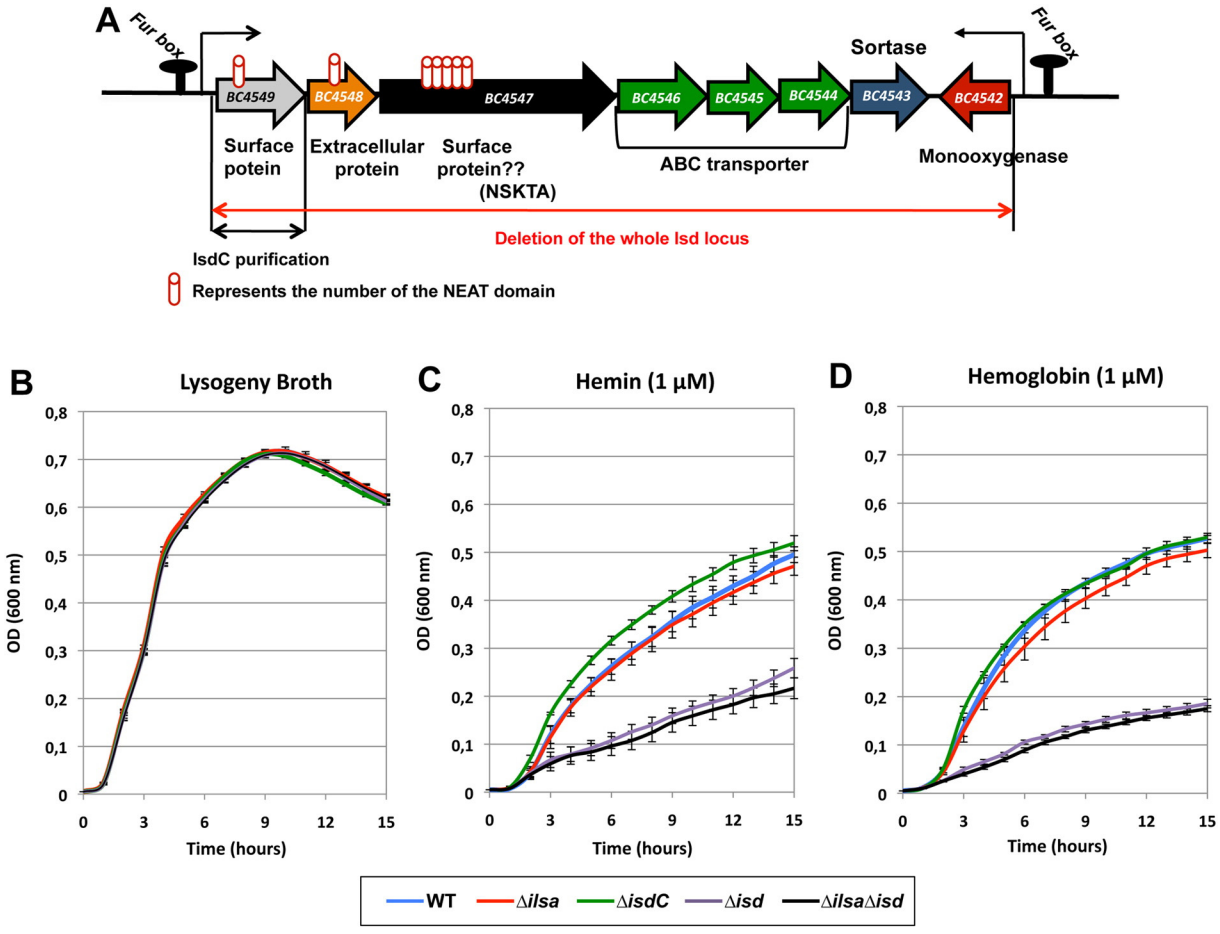


**Fig. 5.** Role of *B. cereus* Isd in heme iron acquisition. (A) The *B. cereus isd* locus showing 8 open reading frames, three NEAT domain proteins: Bc4549, Bc4548, Bc4547, an ABC membrane transporter, Bc4546, Bc4545 and Bc4544, a sortase: Bc4543 and a monooxygenase: Bc4542. (B to D) Growth kinetics studies were conducted with *B. cereus* wild-type (WT) (blue curve), Δ*isdC* (green curve), Δ*isd* (purple curve), Δ*ilsa* (red curve) and Δ*ilsa*Δ*isd* (black curve). The strains were grown at 37 °C in (B) LB medium, (C) iron-treated LB medium and supplemented with 1 µM hemin or (D) 1 µM hemoglobin. Bacterial growth was monitored at 600 nm for 15 h and the curves are averages of 6 independent experiments (error bars are SEM from mean values) and statistical analysis were run with JMP9 SAS software and are shown in Table S1.

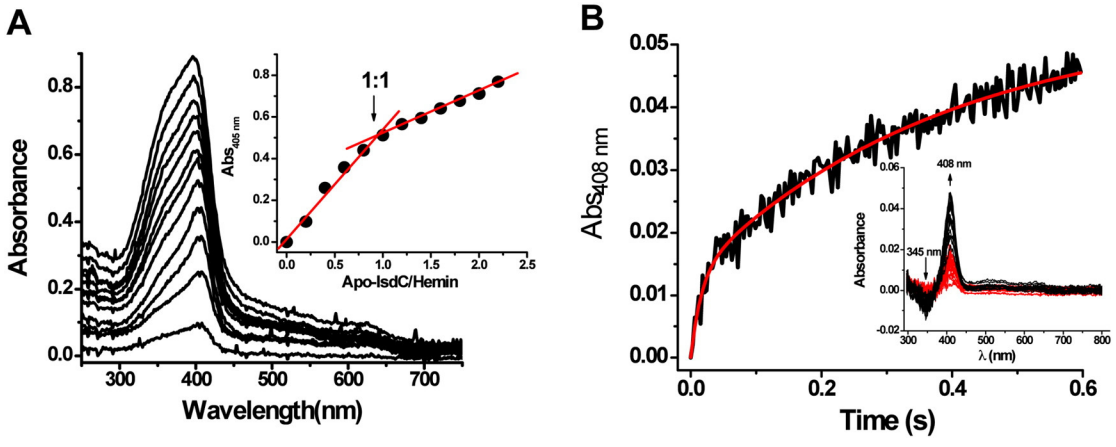


C

| Apo-protein + Hemin | $A_1$ | $k_1$ ( $s^{-1}$) | $A_2$ | $k_2$ ( $s^{-1}$) |
|---|---|---|---|---|
| Apo-IsdC | 0.0134 ± 0.0024 | 58.9± 6.2 | 0.0413 ± 0.0054 | 5.7 ± 0.5 |

**Fig. 6.** Exogeneous hemin binding to apo-IsdC. (A) Spectrophotometric titrations of apo-IsdC (5 µM) with 1 µM hemin per injection. The inset shows the titration curve. (B) Kinetic trace for hemin (7.5 µM) association with apo-IsdC (10 µM) measured with the stopped-flow technique. The red curve is the best fit to the experimental data in black using two exponential equations. The inset of panel B represents the family of spectra gathered every 2.5 ms for the first 50 ms (red) of the reaction and every 20 ms (black) thereafter. (C) First order rate constants ($k_1$ and $k_2$) and the corresponding absorbance values ($A_1$ and $A_2$). All solutions were in 50 mM Tris, 150 mM NaCl, pH 7.4 and 25 °C.

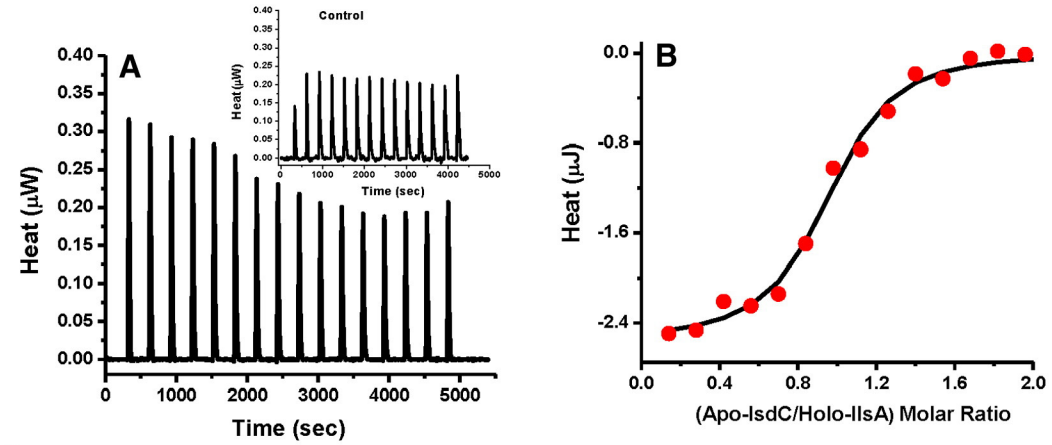


C

| | n (stoichiometry) | K ($M^{-1}$) | ΔH° (KJ/mol) | [a]ΔG° (KJ/mol)[a] | [b]ΔS° (J/K mol)[b] |
|---|---|---|---|---|---|
| Apo-IsdC binding to holo-IlsA | 1.1 ± 0.2 | (3.2 ± 0.8) x$10^6$ | - 8.21 ± 1.35 | -37.09 ± 0.93 | 96.8 ± 5.49 |

[a] Calculated from $\Delta G^0 = -RT \ln K$
[b] Calculated from $\Delta S^0 = (\Delta H^0 - \Delta G^0)/T$

**Fig. 7.** Isothermal titration calorimetry (ITC) of apo-IsdC binding to holo-IlsA. Holo-IlsA (15 μM) is titrated with 3 μl injections of apo-IsdC (109 μM) in 50 mM Tris/HCl buffer, 150 mM NaCl, 1 mM EDTA and 1 mM DTT, pH 7.0 and 25 °C. (A) ITC raw data. (B) Plot of the integrated heat versus the molar ratio of apo-IsdC to holo-IlsA and best fit to the data. (C) ITC thermodynamic parameters for apo-IsdC binding to holo-IlsA. At least three independent determinations were made and the standard deviation of fitted parameters is provided. Additions of apo-IlsA to apo-IsdC yielded heats similar to the control experiment suggesting that heme is required for the association of holo-IlsA to apo-IsdC.

protein, and HasR, an outer membrane receptor protein in the Gram-negative bacterium *Serratia marcescens* showed dissociation constants of 200 nM and 20 nM for HasR-heme and apoHasR-holoHasA, respectively [26]. Other heme transfer measurements between the NEAT domains of holo-IsdB and apoIsdA of the bacterial pathogen *S. aureus* found a protein–protein dissociation constant of 11 μM [16]. Thus, although our ITC experiments cannot differentiate between the relative heat contribution due to hemin transfer from holo-IlsA to apo-Isd and that due to the interaction between apo-IsdC and holo-IlsA, the data, nonetheless, indicate an association between apo-IsdC and hemin-bound IlsA suggesting a role for IsdC in hemin transfer.

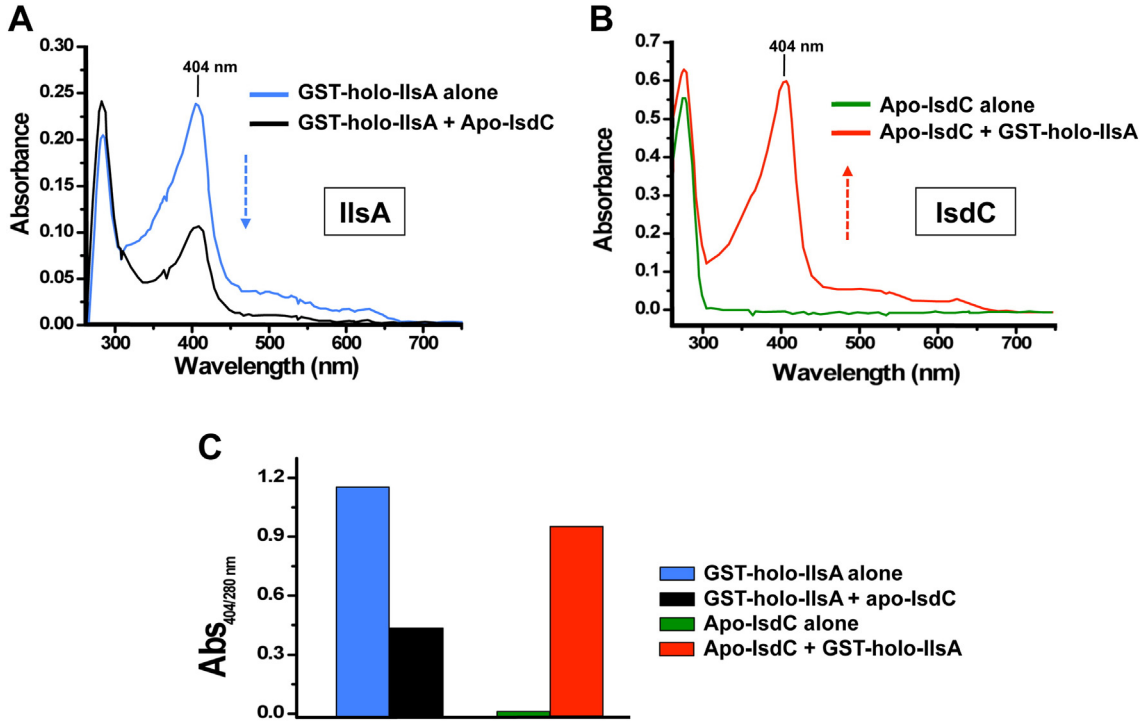


**Fig. 8.** Hemin transfer from holo-IlsA to apo-IsdC. GST-apo-IlsA (10 μM) was loaded onto a glutathione–sepharose gel, charged by hemin and then incubated with apo-IsdC (50 μM) for 30 min at 25 °C. Supernatant and sediment were separated by centrifugation and GST-IlsA was collected by elution with reduced glutathione. The fractions containing (A) IlsA and (B) IsdC were analyzed by UV–Vis and (C) the hemin content was quantified using the 404/280 ratio.

### 2.8. IlsA-bound hemin can be transferred to IsdC

#### 2.8.1. Affinity chromatography of hemin transfer from holo-IlsA to apo-IsdC and vice versa

The ITC results suggest a favorable interaction between holo-IlsA and apo-IsdC. Because both proteins have been shown to bind hemin, we sought to investigate whether hemin can be exchanged between these NEAT domain molecules. Affinity chromatography using glutathione–sepharose gel was used to follow hemin transfer from holo-IlsA to apo-IsdC. Following incubation of apo-IsdC with GST-holo-IlsA, the sediment containing GST-IlsA protein showed a clear decrease at 404 nm (Fig. 8A) while the supernatant containing IsdC protein exhibited a concurrent increase in the absorbance at the same wavelength (Fig. 8B). Analysis of GST-IlsA hemin content (calculated via $A_{404\ nm}/A_{280\ nm}$ ratio) revealed that nearly 60% of hemin-loaded IlsA was transferred to apo-IsdC (Fig. 8C). Interestingly, when the experiment was run with holo-GST-IsdC, only about 20% of hemin was transferred from holo-IsdC to apo-IlsA (Fig. S2). These results suggest that hemin transfer is essentially unidirectional, that holo-IlsA is able to transfer more efficiently its hemin to apo-IsdC and that these two heme-binding proteins interact to assist in heme transfer at the bacterial surface.

### 2.9. Kinetics of hemin transfer from holo-IlsA and holo-$NEAT_{IlsA}$ to apo-IsdC

In order to better characterize the role of IlsA and NEAT domain in hemin transfer from holo-IlsA to apo-IsdC, we followed the kinetics of hemin transfer from three holo-IlsA variants to apo-IsdC. The first variant was purified from heme producing *E. coli* M15 (holo-IlsA M15) while the other two variants, holo-IlsA C600 and holo-$NEAT_{IlsA}$ were purified from heme mutant *E. coli* C600 and were later loaded with exogenous hemin. Hemin transfer was then followed by stopped-flow spectrophotometry at pH 7.4 and 25.0 °C (Fig. 9). The spectral changes at 405 nm, 407 nm and 390 nm are associated with hemin loss from holo-IlsA M15, holo-IlsA C600 and holo-$NEAT_{IlsA}$ while those at 426 nm, 435 nm and 424 nm are attributed to hemin transfer to apo-IsdC, respectively. The hemin dissociation and association rate constants were obtained from fits to the data using single exponential equations and are reported in Fig. 9D. In the presence of apo-IsdC the rate of hemin dissociation from holo-$NEAT_{IlsA}$ ($9.9 \pm 1.1\ s^{-1}$) is about 2-fold faster than that from holo-IlsA C600 ($4.3 \pm 0.9\ s^{-1}$) but similar to holo-IlsA M15 ($7.9 \pm 2.0\ s^{-1}$). In contrast, the pseudo first-order rate constant for hemin association with apo-IsdC is independent of the nature of hemin donor and is similar ($5.9 \pm 0.4\ s^{-1}$ to $7.1 \pm 2.6\ s^{-1}$) among the three holo-IlsA samples tested. These results suggest that the NEAT domain alone is able to transfer hemin as efficiently as the full-length IlsA. The absorbance value of the IsdC-hemin complex formed from $NEAT_{IlsA}$ as hemin donor is on average about four times higher than the IsdC-hemin complex formed from full-length IlsA. The rapid kinetics of hemin transfer from holo-IlsA to IsdC indicate that this process may be mediated by protein–protein interaction [27] as also suggested by the ITC binding data.

*In conclusion*, we demonstrate that IlsA and IsdC from *B. cereus* are capable of binding and exchanging hemin through a dynamic interplay mediated by their NEAT domains. Such protein domains have been shown to have a wide range of functions including hemoglobin binding or heme extraction through direct transfer from hemoglobin to the target protein [28–30,22,31,32]. In recent years, the mechanism of heme transfer in Gram-positive bacteria has gained considerable attention [33–38] in an effort to develop drugs or vaccines for therapeutic targets. In an earlier study, Tarlovsky et al. [27] demonstrated an efficient heme transfer from the BslK protein that harbors a NEAT domain to IsdC (*B. anthracis*). However, the deletion of *bslK* does not render *B. anthracis* unable to grow on heme or hemoglobin as sole iron sources [23]. In the case of IlsA, our results suggest a rapid hemin transfer between two structurally distinct surface proteins, a NEAT-LRR protein (IlsA) and a NEAT-protein (IsdC) belonging to the Isd system. Interestingly a recent study (Honsa et al. 2014) shows that IsdC NEAT domain is a highly conserved structure among Gram positive host associated bacteria, highlighting an important role of this domain in heme binding [46]. Altogether, our study provides new information about the interplay between two different bacterial proteins involved in iron acquisition from heme. Additional work and more structural studies are

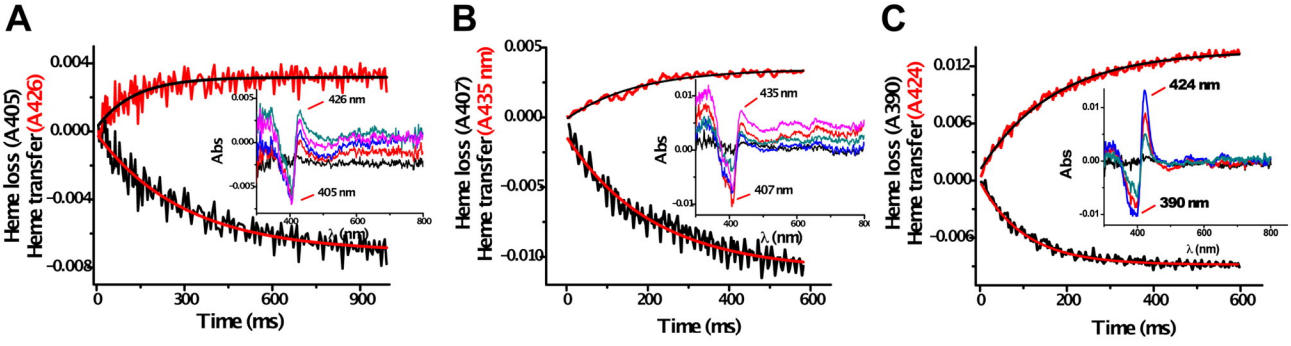


**D**

| Holo-proteins + apo-IsdC | $A_1$ | $k_1$ ($s^{-1}$) 1st order rate cte of hemin dissociation from holo-IlsA | $A_2$ | $k_1$ ($s^{-1}$) pseudo 1st order rate cte of hemin uptake by apo-Isd |
|---|---|---|---|---|
| Holo-IlsA M15 | 0.0048 ± 0.0004 | 7.9 ± 2.0 | 0.0032 ± 0.0013 | 7.1± 2.6 |
| Holo-IlsA-C600 | 0.0096 ± 0.0011 | 4.3 ± 0.9 | 0.0035 ± 0.0005 | 6.4 ± 1.4 |
| Holo-IlsA-NEAT | 0.0087 ± 0.0005 | 9.9 ± 1.1 | 0.0121 ± 0.0005 | 5.9 ± 0.4 |

**Fig. 9.** Kinetics of hemin transfer from holo-IlsA to apo-IsdC. (A) Apo-IsdC (50 μM) was rapidly mixed in a stopped-flow apparatus with holo-IlsA (10 μM, purified from *E. coli* strain M15), (B) holo-IlsA (10 μM, purified from strain C600 Δ*hemA*) and (C) holo-$NEAT_{IlsA}$ (10 μM). The insets represent the family of spectra of hemin loss from holo-IlsA (M15), holo-IlsA (C600) and holo-$NEAT_{IlsA}$ at various times. All protein solutions were in 50 mM Tris, 150 mM NaCl, pH 7.4. (D) First order rate constants (k1) and the corresponding absorbance values (A1 and A2) for hemin transfer from holo-IlsA and holo-$NEAT_{IlsA}$ to apo-IsdC.

needed to elucidate whether other heme-rich molecules like myoglobin, haptoglobin, hemopexin can interact with IlsA and to fully explore the function(s) of IlsA domains.

## 3. Materials and Methods

### 3.1. Homology modeling of IlsA and heme docking in IlsA

The fasta sequence of *Bacillus cereus* IlsA (IlsA_Bc) was retrieved from the UniProtKB server at http://www.uniprot.org/uniprot/ with the entry code Q81G77_BACCR. Using ClustalW (http://www.ebi.ac.uk/Tools/msa/clustalw2/) and (http://npsa-pbil.ibcp.fr/cgi-bin/npsa), the fasta sequence of IlsA_Bc was 2D aligned with IsdA_Sa, IsdB-N2_Sa, and IsdX2_Ba, the homologous Isd proteins in *S. aureus* (Sa) and *B. anthracis* (Ba), respectively, whose fasta sequences were retrieved from their solved structures at http://www.rcsb.org/pdb. These sequences were then 3D aligned using the advanced method in ESPript (http://espript.ibcp.fr/ESPript/ESPript/) to include the secondary features of IsdA_Sa, IsdB-N2_Sa, IsdX2_Ba from their pdb codes: 2ITF, 3RTL and 4H8P, respectively [39]. Hundreds of structures of IlsA_Bc were homology modeled with the three solved X-ray structures cited above as 3D templates and using the model-building software Modeller (mod9v10) to satisfy the spatial restraints issued from the alignment with the target proteins [40]. The model with the lowest score function value and best stereochemistry was selected and superimposed to the three templates that harbored the heme molecule in the binding pocket. The structures, templates, and homology model were then subjected to further refinement by energy minimization using CHARMM implemented in Discovery Studio 2.5 ©, 5000 iterations using Smart algorithm, constraints on the protein backbone and 0.01 RMS (RMS = Root Mean Square deviation refers to an estimate of the statistical deviation, counting all atoms between conformations n − 1 and n. The value 0.01 is a stop criterion and refers to the difference in Angstrom between two structures) gradient as stop criterion [41]. After optimization, the binding energy between the protein and the heme was calculated using the Calculate Energy Interaction module, implemented in Discovery Studio 2.5 ©.

### 3.2. Bacterial strains and growth conditions

*Bacillus cereus* strain ATCC 14579 (laboratory stock) was used throughout this study. *E. coli* K12 strain TG1 was used as a host for cloning experiments. *E. coli* strain ET 12567 (laboratory stock) was used to generate non-methylated DNA for electro-transformation in *B. cereus* as previously described [42,43]. *E. coli* M15 (pREP 4, Km resistant) strain was used for expression and purification of the Glutathione S-transferase (GST) fusion protein (GST-IlsA, GST-IsdC with endogenous heme, $IlsA_{Y147AY151A}$ and LRR domain). The *E. coli* C600 Δ*hemA :: Km* [44] was used to produce the apo-IlsA, apo-$NEAT_{IlsA}$ and apo-IsdC. *E. coli* and *B. cereus* were cultured in LB (Lysogeny Broth) broth, with vigorous shaking (175 rpm) at 37 °C. For electro-transformation, *B. cereus* was grown in BHI (Brain Heart Infusion, Difco) broth. *E. coli* C600 Δ*hemA* was cultured in BHI without shaking. Antibiotics for bacterial selection were used at the following concentrations: ampicillin 100 μg/ml (for *E. coli* TG1 and ET), ampicillin 100 μg/ml + kanamycin 25 μg/ml (for *E. coli* M15), ampicillin 100 μg/ml + kanamycin 20 μg/ml (for *E. coli* C600 Δ*hemA*), and erythromycin 10 μg/ml (for *B. cereus*). The iron chelator 2,2′-dipyridyl and the iron sources, human hemoglobin (Sigma, H7379) and bovine hemin (Sigma, H9039) were purchased from Sigma-Aldrich (Saint Quentin, Fallavier Cedex, France). The possibility that human hemoglobin is a mixture of oligomeric states including normal oxyhemoglobin and methemoglobin where the iron in the heme group is either in the +2 (ferrous) or +3 (ferric) states, respectively, is not precluded in the present work. The concentration of the hemoglobin solution was verified at 280 nm using a molar extinction coefficient of 132000 $M^{-1}$ $cm^{-1}$ for the oxyhemoglobin, assuming hemoglobin is a tetramer predominantly present in the oxidized form. Hemin solutions were prepared accordingly to Ekworomadu et al. [19] "Approximately 4 mg of hemin was dissolved in 0.4 ml of ice cold 0.1 M NaOH and periodically vortexed. After 30 min, 0.4 ml of 1 M Tris, pH 7.4 was added to the solution which was then centrifuged for 10 min at 4 °C and 13,000 rpm. The hemin solution was then diluted with 50 mM Tris, pH 7.4, 150 mM NaCl and centrifuged again at 5,000 rpm to remove any hemin aggregates. Final concentrations were determined at 385 nm using a molar extinction coefficient of 58440 $M^{-1}$ $cm^{-1}$. Hemin solutions were used within 12 h of preparation". Stock concentrations of hemoglobin solutions (20 μM) were prepared in 50 mM Tris, 150 mM NaCl, pH 7.4 and diluted down to 1 μM or 5 μM as indicated in the figure captions.

### 3.3. Production of full-length IlsA, NEAT domain ($NEAT_{IlsA}$), LRR domain ($LRR_{IlsA}$) and IsdC

The *ilsA*, $NEAT^{ilsA}$, $LRR^{ilsA}$ and *isdC* coding sequences were amplified by PCR using genomic DNA from *B. cereus* as template and the following primers F-IlsA prot/R-IlsA prot, F-NEAT IlsA/R-NEAT IlsA, F-LRR/R-LRR and F-IsdC/R-IsdC, respectively (Table S2). The *ilsA*, $NEAT^{ilsA}$, $LRR^{ilsA}$ and *isdC* DNA sequences were digested with EcoRI and XhoI and cloned into the plasmid pGEX-6p-1 holding the tag encoding Glutathione-S Transferase (GST). Analysis of the full-length IlsA protein sequence with the SIGNALP 3.0 program identified a signal peptide cleavage site between amino acid residues 1 and 28 [7]. The DNA sequence corresponding to the signal peptide of IlsA was omitted for the production of the recombinant IlsA (amino acids Ala 29 to Lys 760). Therefore, the soluble protein was produced into the cytosol which facilitated its purification. DNA encoding the NEAT domain (Thr 24 to Gly 163) and the LRR domain (Lys 208 to Asn 493) of IlsA were respectively fused to the DNA encoding GST in pGEX-6p-1 to create pGST-$NEAT_{IlsA}$ and pGST-$LRR_{IlsA}$. Purified IsdC was lacking both the N-terminus signal peptide (amino acids 1–31) and the C-terminus charged tail (amino acids 212–237). All clones were verified by sequencing (Beckman Coulter Genomics, Essex, UK) to rule out spurious mutations. The accession numbers of IlsA and IsdC proteins of *B. cereus* are NP_831113 and NP_834256, respectively.

### 3.4. Site-directed mutagenesis of $NEAT_{IlsA}$ domain

Site-directed mutagenesis of two conserved IlsA tyrosine residues (Tyr 147 and Tyr 151) was performed using the Phusion High-Fidelity DNA polymerase (New England, BioLabs), pGST-IlsA as template and F-Y147AY151A, R-Y147AY151A as primers (Table S2). The PCR products were treated with DpnI (Biolabs) for 1 h at 37 °C to degrade methylated template DNA and transformed into *E. coli* TG1. The resulting gene was designated $ilsA_{Y147AY151A}$. Mutations were confirmed by sequencing (Beckman Coulter Genomics, Essex, UK).

### 3.5. Purification of IlsA, $IlsA_{Y147AY151A}$, $LRR_{IlsA}$ and IsdC in E. coli strain M15

Genes encoding IlsA, $IlsA_{Y147AY151A}$, $LRR_{IlsA}$ and IsdC were overexpressed in *E. coli* M15. Five liters of LB medium were inoculated with 50 ml of overnight cultures supplemented with 100 μg/ml ampicillin and 25 μg/ml kanamycin. The cultures were grown under agitation at 37 °C to an $OD_{600}$ of 0.8–0.9. The expression of the different protein fusions GST-IlsA, GST-$IlsA_{Y147AY151A}$, GST-$LRR_{IlsA}$ or GST-IsdC was induced by adding 1 mM IPTG (isopropyl β-D-thiogalactopyranoside), and the cultures were first incubated for 3 h at 30 °C and then overnight (16 h) at 15 °C. As the proteins were expressed in the cytosol of M15 (except the GST-$LRR_{IlsA}$), the cultures were centrifuged at 8000 rpm, 4 °C for 15 min and the cell pellets re-suspended in 60 ml PBS (Phosphate Buffered Salin) and 3.5 ml of 20% Triton X-100. A 1.5 ml of a lysozyme solution (50 mg/ml) was added and the bacterial cells were incubated for 15 min at room temperature followed by a

DNase I treatment (200 μl of a 5 mg/ml DNase I at 4 °C for 45 min). The bacteria were lysed on ice by sonication using a Branson sonicator 250 (10 s of sonication for 10 times with an interval of 10 s). Bacterial lysate was centrifuged at 15,000 rpm, for 15 min at 4 °C; soluble proteins from the supernatants were filtered through 0.22 μm pore size filter (Millipore). Since the GST-$LRR_{IlsA}$ fusion protein was localized in the pellet, solubilization was achieved by overnight incubation at 4 °C in 80 ml Tris buffer (50 mM, pH 8.0) containing 8 M urea at 4 °C. The insoluble pellet was removed by centrifugation at 8000 rpm for 45 min at 4 °C. The supernatant containing the solubilized protein was dialyzed against 50 mM Tris buffer (pH 8.0) and 1 M urea for approximately 5 h with stirring at 4 °C and then against the same buffer without urea for nearly 48 h with stirring at 4 °C to remove the residual chaotropic agent. The filtrate containing the tagged GST-proteins and the solubilized GST-$LRR_{IlsA}$ were incubated overnight at 4 °C with agitation in the presence of 3.3 ml of Glutathione Sepharose 4B (GE Healthcare).

The affinity gel holding the target protein was loaded onto a column and washed with 75 ml PBS (1×) and then 50 ml of the PreScission protease buffer (50 mM Tris–HCl pH 7.0, 150 mM NaCl, 1 mM EDTA, 1 mM DTT). The GST was cleaved by PreScission proteasefor 16 h at 4 °C. For some set of experiments we kept the GST tag by eluting the gel with the L-Glutathione reduced (Sigma-Aldrich, G4251). The purification of IlsA, $IlsA_{Y147AY151A}$, $LRR_{IlsA}$ and IsdC was monitored by 10% SDS PAGE. IlsA and IsdC proteins were purified with the endogenous hemin from *E. coli* strain M15 whereas the IlsA NEAT domain mutant and the $LRR_{IlsA}$ did not contain hemin. Average yield of purified proteins varied from 5 mg to 10 mg per liter of growth medium.

### 3.6. Purification of IlsA, $NEAT_{IlsA}$ and IsdC in apo-form

The apo forms of IlsA, $NEAT_{IlsA}$ and IsdC proteins were produced in *E. coli* C600 Δ*hemA*: *Km*, a strain knocked out for heme synthesis [44]. The recombinant proteins apo-IlsA, apo-$NEAT_{IlsA}$ and apo-IsdC were expressed in 10 L of BHI (Brain Heart Infusion, Difco) supplemented with 100 μg/ml ampicillin and 20 μg/ml kanamycin. Cultures were grown in bottles without shaking at 37 °C to an $OD_{600}$ of 0.8–0.9. The expression, production and the purification of proteins were performed as described above in *E. coli* M15.

### 3.7. Reconstitution of holo-proteins

The concentration of the proteins purified in *E. coli* M15 were determined either by the Bio-Rad protein assay or spectrophotometrically at 280 nm using molar extinction coefficients (ε) of 60,740 $M^{-1}$ $cm^{-1}$ for apo-IlsA, 12,090 $M^{-1}$ $cm^{-1}$ for apo-IsdC, 10,500 $M^{-1}$ $cm^{-1}$ for apo-$NEAT_{IlsA}$, 57,760 $M^{-1}$ $cm^{-1}$ for $IlsA_{Y147AY151A}$, 103,600 $M^{-1}$ $cm^{-1}$ for GST-apo-IlsA and 50,120 $M^{-1}$ $cm^{-1}$ for GST-apo-$NEAT_{IlsA}$. To reconstitute the holo proteins, hemin was prepared as described above and added stoichiometrically to the apo-proteins. The apo-proteins purified from *E. coli* C600 Δ*hemA* were 80–90% saturated by exogenous hemin.

### 3.8. Hemin binding

Hemin binding to apo-IlsA, apo-IsdC, apo-$NEAT_{IlsA}$ and $IlsA_{Y147AY151A}$ was followed spectrophotometrically at 405 nm using a Varian Cary 50 Bio UV–Vis spectrophotometer and several aliquots of a hemin solution as described in the figure captions. The kinetics of hemin binding to the apo-proteins were measured using a pneumatic drive Hi-Tech SFA-20 M stopped-flow apparatus interfaced to a J&M Tidas diode array spectrometer with data acquisition every 2.5 ms in the wavelength range of 190–1024 nm. Equal 140 μl volumes of hemin (15 or 20 μM) and apo-IlsA (30 μM), apo-$NEAT_{IlsA}$ (30 μM) or apo-IsdC (20 μM) buffered solutions (50 mM Tris, 150 mM NaCl, pH 7.4) were rapidly mixed into the quartz stopped-flow cuvette having a 1 cm path length and a cell volume of 80 μl. All concentrations given in the figure captions are final concentrations following mixing of the reagents.

### 3.9. Heme extraction from hemoglobin

Extraction assays were performed in 1.5 ml eppendorfs tubes. 20 μM of GST-apo-IlsA, 20 μM of GST-apo-$NEAT_{IlsA}$, 10 μM of GST-$LRR_{IlsA}$ or PBS (control) (200 μl) were first mixed with 200 μl glutathione–sepharose for 30 min at 25 °C followed by centrifugation and three washes with 200 μl PBS. Human hemoglobin was added at 5 μM (200 μl) and incubated with the different GST-proteins bound to glutathione–sepharose for 30 min at 25 °C. Mixtures were centrifuged and the supernatant containing hemoglobin was separated from the glutathione–sepharose gel which was washed three times with PBS prior to elution with reduced glutathione (200 μl) to recover the GST-IlsA, GST-$NEAT_{IlsA}$ or GST-$LRR_{IlsA}$. The sediment (containing the GST tagged proteins) and the supernatant (containing hemoglobin) were subjected to spectroscopic measurements and heme binding was evaluated at 405 nm with a UV–Vis spectrophotometer (UV-2501PC, Shimadzu). The experiments were repeated three times and the curves shown in Fig. 1 are a representation of one of the trials. The Hb + apo-protein curves (red spectra) represent the absorbance spectra of hemoglobin remaining in the supernatant after incubation with the GST-apo-proteins bound to the glutathione–sepharose gel. The apo-protein + Hb curves (green spectra) represent the absorbance spectra of the GST-proteins (GST-apo-IlsA, GST-apo-$NEAT_{IlsA}$, and GST-$LRR_{IlsA}$) after dissociation from the glutathione–sepharose gel using glutathione elution buffer. The GST-proteins bound to the glutathione–sepharose gel were first incubated with Hb followed by centrifugation and separation.

### 3.10. Isothermal titration calorimetry (ITC) of holo-IlsA binding to apo-IsdC

The binding interaction between holo-IlsA saturated with bovine hemin and apo-IsdC was followed at 25.00 °C and pH 7.0 in a low reaction cell volume (185 μl) NanoITC from TA Instruments. An automated sequence of 16 injections of 3 μl each of apo-IsdC (109 μM) into the sample cell containing holo-IlsA (15 μM) spaced at 5 min intervals to allow complete equilibration was performed. The data was collected automatically and analyzed with the NanoAnalyze fitting program (provided by TA Instruments) using a mathematical model involving one class of independent binding sites. The ITC experiments were repeated three times with a background correction using the buffer solution alone to account for the heat of dilution. The standard enthalpy change (ΔH°), the binding constant (K) and the stoichiometry of binding (n) were directly determined from each run and the standard Gibbs free energy change (ΔG°) and standard entropy change (ΔS°) were calculated using the following equations: $\Delta G^\circ = -RT\ln K$ and $T\Delta S^\circ = \Delta H^\circ - \Delta G^\circ$. The SD errors from curve fitting given in Fig. 7D are from three replicate measurements. We should mention that all reported thermodynamic quantities in this study are apparent values (i.e. experimentally measured values under non-standard conditions) which include contributions to the overall equilibrium from different processes such as protein conformational changes upon binding, ligands and buffer species in different states of protonation and heme transfer following protein mixing.

### 3.11. Hemin transfer from holo-IlsA to apo-IsdC

A solution of 200 μl of 10 μM GST-apo-IlsA or PBS (control) was coupled to 50 μl of glutathione–sepharose for 30 min at 25 °C. The gel was then washed three times with 200 μl PBS (1×). Bovine hemin was added at a final concentration of 10 μM and incubated for 30 min at 25 °C. The solution was centrifuged and the sediment gel/GST-holo-IlsA complex was washed three times with 200 μl of PBS. 50 μM of apo-IsdC (200 μl) was incubated either with GST-holo-IlsA or PBS for 30 min at 25 °C. The mixture was centrifuged to separate the glutathione–sepharose holding the donor and the supernatant containing the receptor molecule. The sediment was washed 3 times with 200 μl PBS and then eluted with 100 μl of reduced glutathione to recover the

GST-IlsA. Hemin content was quantified by spectrophotometric measurements at 404 nm with a UV–Vis spectrophotometer (UV-2501PC, Shimadzu). The experiment was repeated three times and the curves shown in Fig. 8 are a representation of one of the trials. The kinetics of hemin transfer from holo-IlsA and holo-$NEAT_{IlsA}$ (loaded with endogenous or exogenous hemin) to apo-IsdC were followed by stopped-flow between 250 and 800 nm in 50 mM Tris, 150 mM NaCl, pH 7.4.

### 3.12. Construction of the B. cereus isd locus and isdC mutants

*B. cereus* Δ*isd* was constructed as follows. A 1032 bp EcoRI/PstI DNA fragment and a 1024 bp PstI/BamHI DNA fragment corresponding to the chromosomal regions located upstream and downstream the *isd* operon respectively, were amplified by PCR using *B. cereus* strain ATCC 14579 chromosomal DNA as a template and primers pairs F-Aoperon/R-Aoperon and F-Boperon/R-Boperon respectively (Table S2). The *isdC* mutant was generated by allelic exchange using deletion replacement. An 870 bp and a 913 bp DNA regions upstream and downstream the gene were respectively amplified by PCR using chromosomal DNA of *B. cereus* strain as template and FAisd4549/RAisd4549, FBisd4549/RBisd4549 as primers (Table S2). The resulting DNA fragments were fused by overlapping PCR with the FAisd4549 and RBisd4549 primers. The amplified DNA was digested with the appropriate enzymes and cloned between EcoRI and BamHI sites of the thermosensitive plasmid pMAD, conferring resistance to erythromycin and carrying a thermostable β-galactosidase gene [45]. The resultant plasmids were introduced into the wild type *B. cereus* strain and double-cross-over events resulted, in the deletion of the whole *isd* locus and *isd4549* coding sequences, respectively. The two deletions were performed without insertion of antibiotic resistance cassettes. Therefore, chromosomal allele exchange and gene deletion were checked by PCR using appropriate oligonucleotide primers.

### 3.13. Growth assay of wild type and mutant strains

*B. cereus* strains were grown overnight under low iron conditions by inoculating strains in LB medium supplemented with 200 μM 2,2′-dipyridyl. Overnight cultures were inoculated into a new LB medium containing 200 μM 2,2′-dipyridyl at a final OD of 0,01. Bacteria from mid exponential phase culture were washed twice in LB medium containing 600 μM 2,2′-dipyridyl and then inoculated to a final optical density (OD) of about 0.005 into 100 μl LB medium, LB medium containing 600 μM 2,2′-dipyridyl, or LB medium containing either 1 μM hemoglobin or 1 μM hemin added exogenously. Stock solutions of these two iron sources were pre-treated with 1 mM 2,2′-dipyridyl for three hours to eliminate any free iron that might be present in solution. *B. cereus* cells were grown at 37 °C in 96-wells microtiter plate under continuous shaking. The OD was measured at 600 nm every hour for 15 h using a TECAN Infinite M200 Microplate Reader (TECAN Group, Männedorf, Switzerland). Each assay was repeated six times.

## Transparency document

The Transparency document associated with this article can be found, in the online version.

## Acknowledgments

This work was supported by grants from ANR (Agence Nationale de la Recherche, programme MIE 2009–2013) to the GrabIron project ANR-MIEN 010-01(DS), from INRA (Institut National de la recherche agronomique), Mica Department-France (CNL, EAK), and Conseil de la recherche, Saint Joseph University — Beirut, Lebanon (FS26) (EAK, MK), to ABIES for the travel support (EAK) and by the Cottrell College Science Award (ID # 7892) from the Research Corporation and the National Science Foundation (NSF MRI Award # 0921364) (FBA). The authors are grateful to the members of the GrabIron project teams for their insights and constructive comments and to Michel Gohar for helping with the statistical analysis.

## Appendix A. Supplementary data

Supplementary data to this article can be found online at http://dx.doi.org/10.1016/j.bbagen.2015.06.006.

## References

[1] S.C. Andrews, A.K. Robinson, F. Rodriguez-Quinones, Bacterial iron homeostasis, FEMS Microbiol. Rev. 27 (2–3) (2003) 215–237.
[2] C. Wandersman, P. Delepelaire, Haemophore functions revisited, Mol. Microbiol. 85 (4) (2012) 618–631.
[3] C.L. Nobles, A.W. Maresso, The theft of host heme by Gram-positive pathogenic bacteria, Metallomics 3 (8) (2011) 788–796.
[4] A.B. Kolsto, D. Lereclus, M. Mock, Genome structure and evolution of the *Bacillus cereus* group, Curr. Top. Microbiol. Immunol. 264 (2) (2002) 95–108.
[5] A.B. Kolsto, N.J. Tourasse, O.A. Okstad, What sets *Bacillus anthracis* apart from other *Bacillus* species? Annu. Rev. Microbiol. 63 (2009) 451–476.
[6] G.T. Vilas-Boas, A.P. Peruca, O.M. Arantes, Biology and taxonomy of *Bacillus cereus*, *Bacillus anthracis*, and *Bacillus thuringiensis*, Can. J. Microbiol. 53 (6) (2007) 673–687.
[7] S. Fedhila, N. Daou, D. Lereclus, C. Nielsen-LeRoux, Identification of *Bacillus cereus* internalin and other candidate virulence genes specifically induced during oral infection in insects, Mol. Microbiol. 62 (2) (2006) 339–355.
[8] N. Daou, C. Buisson, M. Gohar, J. Vidic, H. Bierne, M. Kallassy, D. Lereclus, C. Nielsen-LeRoux, IlsA, a unique surface protein of *Bacillus cereus* required for iron acquisition from heme, hemoglobin and ferritin, PLoS Pathog. 5 (11) (2009) e1000675.
[9] E.S. Honsa, A.W. Maresso, Mechanisms of iron import in anthrax, Biometals 24 (3) (2011) 533–545.
[10] B. Kobe, J. Deisenhofer, The leucine-rich repeat: a versatile binding motif, Trends Biochem. Sci. 19 (10) (1994) 415–421.
[11] B. Kobe, A.V. Kajava, When protein folding is simplified to protein coiling: the continuum of solenoid protein structures, Trends Biochem. Sci. 25 (10) (2000) 509–515.
[12] J.C. Grigg, C.L. Vermeiren, D.E. Heinrichs, M.E. Murphy, Haem recognition by a *Staphylococcus aureus* NEAT domain, Mol. Microbiol. 63 (1) (2007) 139–149.
[13] C.F. Gaudin, J.C. Grigg, A.L. Arrieta, M.E. Murphy, Unique heme-iron coordination by the hemoglobin receptor IsdB of *Staphylococcus aureus*, Biochemistry 50 (24) (2011) 5443–5452.
[14] K.H. Sharp, S. Schneider, A. Cockayne, M. Paoli, Crystal structure of the heme-IsdC complex, the central conduit of the Isd iron/heme uptake system in *Staphylococcus aureus*, J. Biol. Chem. 282 (14) (2007) 10625–10631.
[15] E.S. Honsa, C.P. Owens, C.W. Goulding, A.W. Maresso, The near-iron transporter (NEAT) domains of the anthrax hemophore IsdX2 require a critical glutamine to extract heme from methemoglobin, J. Biol. Chem. 288 (12) (2013) 8479–8490.
[16] J.C. Grigg, C.X. Mao, M.E. Murphy, Iron-coordinating tyrosine is a key determinant of NEAT domain heme transfer, J. Mol. Biol. 413 (3) (2011) 684–698.
[17] K.A. de Villiers, C.H. Kaschula, T.J. Egan, H.M. Marques, Speciation and structure of ferriprotoporphyrin IX in aqueous solution: spectroscopic and diffusion measurements demonstrate dimerization, but not mu-oxo dimer formation, J. Biol. Inorg. Chem. 12 (1) (2007) 101–117.
[18] M. Liu, W.N. Tanaka, H. Zhu, G. Xie, D.M. Dooley, B. Lei, Direct hemin transfer from IsdA to IsdC in the iron-regulated surface determinant (Isd) heme acquisition system of *Staphylococcus aureus*, J. Biol. Chem. 283 (11) (2008) 6668–6676.
[19] M.T. Ekworomadu, C.B. Poor, C.P. Owens, M.A. Balderas, M. Fabian, J.S. Olson, F. Murphy, E. Balkabasi, E.S. Honsa, C. He, C.W. Goulding, A.W. Maresso, Differential function of lip residues in the mechanism and biology of an anthrax hemophore, PLoS Pathog. 8 (3) (2012) e1002559.
[20] K.K. Krishna, D.A. Jacques, G. Pishchany, T. Caradoc-Davies, T. Spirig, G.R. Malmirchegini, D.B. Langley, C.F. Dickson, J.P. Mackay, R.T. Clubb, E.P. Skaar, J.M. Guss, D.A. Gell, Structural basis for hemoglobin capture by *Staphylococcus aureus* cell-surface protein, IsdH, J. Biol. Chem. 286 (44) (2011) 38439–38447.
[21] D. Segond, E. Abi Khalil, C. Buisson, N. Daou, M. Kallassy, D. Lereclus, P. Arosio, F. Bou-Abdallah, C. Nielsen Le Roux, Iron acquisition in *Bacillus cereus*: The roles of IlsA and bacillibactin in exogenous ferritin iron mobilization, PLoS Pathog. 10 (2) (2014) e1003935.
[22] A.W. Maresso, T.J. Chapa, O. Schneewind, Surface protein IsdC and Sortase B are required for heme-iron scavenging of *Bacillus anthracis*, J. Bacteriol. 188 (23) (2006) 8145–8152.
[23] A.W. Maresso, G. Garufi, O. Schneewind, *Bacillus anthracis* secretes proteins that mediate heme acquisition from hemoglobin, PLoS Pathog. 4 (8) (2008) e1000132.
[24] M.A. Balderas, C.L. Nobles, E.S. Honsa, E.R. Alicki, A.W. Maresso, Hal is a *Bacillus anthracis* heme acquisition protein, J. Bacteriol. 194 (20) (2012) 5513–5521.
[25] D. Grenier, M.P. Huot, D. Mayrand, Iron-chelating activity of tetracyclines and its impact on the susceptibility of *Actinobacillus actinomycetemcomitans* to these antibiotics, Antimicrob. Agents Chemother. 44 (3) (2000) 763–766.
[26] A. Yamaguchi, T. Udagawa, T. Sawai, Transport of divalent cations with tetracycline as mediated by the transposon Tn10-encoded tetracycline resistance protein, J. Biol. Chem. 265 (9) (1990) 4809–4813.

[27] N. Izadi-Pruneyre, F. Huche, G.S. Lukat-Rodgers, A. Lecroisey, R. Gilli, K.R. Rodgers, C. Wandersman, P. Delepelaire, The heme transfer from the soluble HasA hemophore to its membrane-bound receptor HasR is driven by protein–protein interaction from a high to a lower affinity binding site, J. Biol. Chem. 281 (35) (2006) 25541–25550.
[28] Y. Tarlovsky, M. Fabian, E. Solomaha, E. Honsa, J.S. Olson, A.W. Maresso, A *Bacillus anthracis* S-layer homology protein that binds heme and mediates heme delivery to IsdC, J. Bacteriol. 192 (13) (2010) 3503–3511.
[29] S.K. Mazmanian, E.P. Skaar, A.H. Gaspar, M. Humayun, P. Gornicki, J. Jelenska, A. Joachmiak, D.M. Missiakas, O. Schneewind, Passage of heme-iron across the envelope of *Staphylococcus aureus*, Science 299 (5608) (2003) 906–909.
[30] V.J. Torres, G. Pishchany, M. Humayun, O. Schneewind, E.P. Skaar, *Staphylococcus aureus* IsdB is a hemoglobin receptor required for heme iron utilization, J. Bacteriol. 188 (24) (2006) 8421–8429.
[31] R.M. Pilpa, E.A. Fadeev, V.A. Villareal, M.L. Wong, M. Phillips, R.T. Clubb, Solution structure of the NEAT (NEAr Transporter) domain from IsdH/HarA: the human hemoglobin receptor in *Staphylococcus aureus*, J. Mol. Biol. 360 (2) (2006) 435–447.
[32] A. Dryla, D. Gelbmann, A. von Gabain, E. Nagy, Identification of a novel iron regulated staphylococcal surface protein with haptoglobin–haemoglobin binding activity, Mol. Microbiol. 49 (1) (2003) 37–53.
[33] A. Dryla, B. Hoffmann, D. Gelbmann, C. Giefing, M. Hanner, A. Meinke, A.S. Anderson, W. Koppensteiner, R. Konrat, G.A. von, E. Nagy, High-affinity binding of the staphylococcal HarA protein to haptoglobin and hemoglobin involves a domain with an antiparallel eight-stranded beta-barrel fold, J. Bacteriol. 189 (1) (2007) 254–264.
[34] M. Fabian, E. Solomaha, J.S. Olson, A.W. Maresso, Heme transfer to the bacterial cell envelope occurs via a secreted hemophore in the Gram-positive pathogen *Bacillus anthracis*, J. Biol. Chem. 284 (46) (2009) 32138–32146.
[35] H. Zhu, G. Xie, M. Liu, J.S. Olson, M. Fabian, D.M. Dooley, B. Lei, Pathway for heme uptake from human methemoglobin by the iron-regulated surface determinants system of *Staphylococcus aureus*, J. Biol. Chem. 283 (26) (2008) 18450–18460.
[36] N. Muryoi, M.T. Tiedemann, M. Pluym, J. Cheung, D.E. Heinrichs, M.J. Stillman, Demonstration of the iron-regulated surface determinant (Isd) heme transfer pathway in *Staphylococcus aureus*, J. Biol. Chem. 283 (42) (2008) 28125–28136.
[37] M. Liu, B. Lei, Heme transfer from streptococcal cell surface protein Shp to HtsA of transporter HtsABC, Infect. Immun. 73 (8) (2005) 5086–5092.
[38] H. Zhu, M. Liu, B. Lei, The surface protein Shr of *Streptococcus pyogenes* binds heme and transfers it to the streptococcal heme-binding protein Shp, BMC. Microbiol. 8 (2008) 15.
[39] P. Gouet, E. Courcelle, D.I. Stuart, F. Metoz, ESPript: analysis of multiple sequence alignments in PostScript, Bioinformatics 15 (4) (1999) 305–308.
[40] N. Eswar, B. Webb, M.A. Marti-Renom, M.S. Madhusudhan, D. Eramian, M.Y. Shen, U. Pieper, A. Sali, Comparative protein structure modeling using Modeller, *Current Protocols in Bioinformatics* (2006) 15:5.6:5.6.1–5.6.30 (Chapter 5, Unit 5.6).
[41] B.R. Brooks, C.L. Brooks III, A.D. Mackerell Jr., L. Nilsson, R.J. Petrella, B. Roux, Y. Won, G. Archontis, C. Bartels, S. Boresch, A. Caflisch, L. Caves, Q. Cui, A.R. Dinner, M. Feig, S. Fischer, J. Gao, M. Hodoscek, W. Im, K. Kuczera, T. Lazaridis, J. Ma, V. Ovchinnikov, E. Paci, R.W. Pastor, C.B. Post, J.Z. Pu, M. Schaefer, B. Tidor, R.M. Venable, H.L. Woodcock, X. Wu, W. Yang, D.M. York, M. Karplus, CHARMM: the biomolecular simulation program, J. Comput. Chem. 30 (10) (2009) 1545–1614.
[42] W.J. Dower, J.F. Miller, C.W. Ragsdale, High efficiency transformation of *E. coli* by high voltage electroporation, Nucleic Acids Res. 16 (13) (1988) 6127–6145.
[43] D. Lereclus, O. Arantes, J. Chaufaux, M. Lecadet, Transformation and expression of a cloned delta-endotoxin gene in *Bacillus thuringiensis*, FEMS Microbiol. Lett. 51 (1) (1989) 211–217.
[44] J.M. Ghigo, S. Letoffe, C. Wandersman, A new type of hemophore-dependent heme acquisition system of *Serratia marcescens* reconstituted in *Escherichia coli*, J. Bacteriol. 179 (11) (1997) 3572–3579.
[45] M. Arnaud, A. Chastanet, M. Debarbouille, New vector for efficient allelic replacement in naturally nontransformable, low-GC-content, gram-positive bacteria, Appl. Environ. Microbiol. 70 (11) (2004) 6887–6891.
[46] E.S. Honsa, A.W. Maresso, S.K. Highlander, Molecular and *Evolutionary Analysis* of NEAr-iron Transporter (NEAT) domains, PLoS One 9 (8) (2014) e104794.